Supplementary Information

I. Tight-binding parameters for CHC-1 (CHC-1')

The sp^3 dimer atoms in CHC-1 decrease the symmetry of the structure, which complicates the bond lengths between atoms. The primitive cell of CHC-1 has 12 sp^2 atoms, and these atoms can be divided into 4 layers along *c* axis according to the colors. The atoms in the primitive cell form a triangle in each layer, as shown in Figs. S2(a-b). The structure has an inversion symmetry, and thus the first (second) layer is equal to the fourth (third) layer. However, the first layer is different from the second layer. The intra- and inter-layer bond lengths also depend on the layers. Therefore, there are multiple hopping energies between atoms. To describe the atomic interactions by the hopping parameters, based on t_i (i=0~5), we define $t_{i/mn}$ (i=0~5, m, n=1~4), where m and n label the ordinal number of layers. For instance, in Figs. S2(a) and S2(b), we present two examples for t_0 and t_1. All the hopping parameters vary with the bond lengths. In Table S2, the corresponding hopping energies for CHC-1 and CHC-1' are shown. Figure S2(c) shows the band structure of CHC-1 according to the values given in the last column of Table S2. One can find that these parameters reproduce the DFT band structure in Fig. S1(a).

II. $\mathbf{k}\cdot\mathbf{p}$ model for CHC-1 (CHC-1')

We assume a three-band model expanded in the vicinity of the k_z axis for a system having time-reversal (complex conjugation *K*), inversion (*I*), mirror (M_y), and 3-fold rotation (C_3^z) symmetries. The three basis states will be denoted as $|1\rangle=|v_-\rangle$, $|2\rangle=|v_+\rangle$, and $|3\rangle=|v_0\rangle$. For a heuristic picture, we can imagine that these have the same symmetries as $|p_y\rangle+i|p_x\rangle$, $|p_y\rangle-i|p_x\rangle$, and $|s\rangle$ respectively, where $|p_x\rangle$ and $|p_y\rangle$ refer to *p* orbitals and $|s\rangle$ is an *s* orbital, although our actual basis orbitals are more complicated linear combinations of atomic orbitals in the layered structure. The 3×3 matrix $H_{ij}(\boldsymbol{k})$ is Hermitian for any $\boldsymbol{k}$, i.e., $H_{ji}(\boldsymbol{k})= H_{ij}^*(\boldsymbol{k})$.

Regarding inversion symmetry *I*, the orbitals are assumed to transform as $I|v_-\rangle=-|v_-\rangle$, $I|v_+\rangle=-|v_+\rangle$, and $I|v_0\rangle=|v_0\rangle$. Inversion takes $\mathrm{k}\rightarrow-\mathrm{k}$ in addition, so it follows that $H_{ij}(\boldsymbol{k})=H_{ij}(-\boldsymbol{k})$ for *ij*=11, 22, 33, and 12, while $H_{ij}(\boldsymbol{k})=-H_{ij}(-\boldsymbol{k})$ for *ij*=13 and 23.

Regarding time reversal symmetry K, the orbitals are assumed to transform as K $|v_-\rangle=|v_+\rangle$, K $|v_+\rangle=|v_-\rangle$, and K $|v_0\rangle=|v_0\rangle$. TR also takes $\mathrm{k}\rightarrow-\mathrm{k}$, and is antiunitary, so it follow that $H_{11}(\boldsymbol{k})=H_{22}(-\boldsymbol{k})$, $H_{33}(\boldsymbol{k})=H_{33}(-\boldsymbol{k})$, $H_{12}(\boldsymbol{k})=H_{12}(-\boldsymbol{k})$, and $H_{13}(\boldsymbol{k})= H_{23}^*(\boldsymbol{k})$.

Regarding rotational symmetry C_3^z, the orbitals transform are assumed to transform as $C_3^z|v_-\rangle=\gamma|v_-\rangle$, $C_3^z|v_+\rangle=\gamma^2|v_+\rangle$, and $C_3^z|v_0\rangle=|v_0\rangle$, where $\gamma=\mathrm{e}^{2\pi\mathrm{i}/3}$. C_3^z also takes $\mathrm{k}_-\rightarrow\gamma\mathrm{k}_-$, $\mathrm{k}_+\rightarrow\gamma^2\mathrm{k}_+$, and $\mathrm{k}_0\rightarrow\mathrm{k}_0$. Thus, if an element in the Harmiltonian matrix has a term of the form $\mathrm{k}_-^{\mathrm{m}-}\mathrm{k}_+^{\mathrm{m}+}$ then $\mathrm{m}_+-\ \mathrm{m}_-=2$ mod 3 for H_{13}.

With all of these constraints, we can systematically write the Hamiltonian matrix up to overall quadratic order in $\mathrm{k_z}$ and $\mathrm{k_y}$ as

$$\mathrm{H(k)} = \begin{pmatrix} \mathrm{a(k_z)} + \mathrm{b(k_z)k_\parallel^2} & \mathrm{e'(k_z)k_+} + \mathrm{f(k_z)k_-^2} & \mathrm{g(k_z)k_-} + \mathrm{h'(k_z)k_+^2} \\ \mathrm{e'(k_z)k_-} + \mathrm{f(k_z)k_+^2} & \mathrm{a(k_z)} + \mathrm{b(k_z)k_\parallel^2} & -\mathrm{g(k_z)k_+} + \mathrm{h'(k_z)k_-^2} \\ \mathrm{g(k_z)k_+} + \mathrm{h'(k_z)k_-^2} & \mathrm{g(k_z)k_-} + \mathrm{h'(k_z)k_+^2} & \mathrm{c(k_z)} + \mathrm{d(k_z)k_\parallel^2} \end{pmatrix}$$

where $\mathrm{k_\parallel^2} = \mathrm{k_+k_-} = \mathrm{k_x^2} + \mathrm{k_y^2}$, and real $\mathrm{a(k_z)}$ etc. are even functions of $\mathrm{k_z}$ if they do not carry a prime and odd if they do.

Finally, we construct a minimal model by letting the odd functions of k_z take the form $\sin k_z$ and even ones being $\cos k_z$ plus a constant. Also dropping the quadratic tem involving $\mathrm{h'(k_z)}$ and renaming the coefficients, we obtain the model

$$\mathrm{H(k)} = \begin{pmatrix} \mathrm{A_1k_\parallel^2} + \mathrm{B_1}\cos\mathrm{k_z} + \mathrm{C_1} & \alpha\mathrm{k_+}\sin\mathrm{k_z} + \beta\mathrm{k_-^2} & \mathrm{Dk_-} \\ \alpha\mathrm{k_-}\sin\mathrm{k_z} + \beta\mathrm{k_+^2} & \mathrm{A_1k_\parallel^2} + \mathrm{B_1}\cos\mathrm{k_z} + \mathrm{C_1} & -\mathrm{Dk_+} \\ \mathrm{Dk_+} & -\mathrm{Dk_-} & \mathrm{A_2k_\parallel^2} + \mathrm{B_2}\cos\mathrm{k_z} + \mathrm{C_2} \end{pmatrix}, \quad (1)$$

that was introduced earlier in the main text.

Equation (1) can be simplified to the following form,

$$\mathrm{H(k)} = \begin{pmatrix} \mathrm{Ak_\parallel^2} + \mathrm{B}\cos\mathrm{k_z} & \alpha\mathrm{k_+}\sin\mathrm{k_z} + \beta\mathrm{k_-^2} & \mathrm{Dk_-} \\ \alpha\mathrm{k_-}\sin\mathrm{k_z} + \beta\mathrm{k_+^2} & A\mathrm{k_\parallel^2} + \mathrm{B}\cos\mathrm{k_z} & -\mathrm{Dk_+} \\ \mathrm{Dk_+} & -\mathrm{Dk_-} & -\mathrm{Ak_\parallel^2} - B\cos\mathrm{k_z} \end{pmatrix}. \quad (2)$$

By solving Eq. (2), one can obtain the three analytic energy eigenvalues $\mathrm{E_1}$, $\mathrm{E_2}$ and $\mathrm{E_3}$. Then, the nodal line should satisfy $\mathrm{E_1} = \mathrm{E_2}$, i.e.,

$$(\beta\mathrm{k_x^2} + \alpha k_x \sin\mathrm{k_z})[(2(A\mathrm{k_x^2} + B\cos\mathrm{k_z}) + (\beta\mathrm{k_x^2} + \alpha k_x \sin\mathrm{k_z})] = D^2\mathrm{k_x^2}. \quad (3)$$

It has four solutions, one of which is $k_x = 0$, corresponding to the straight nodal line along k_z. The other three correspond to the hybrid nodal lines on the plane $k_y = 0$. By tuning the parameters α and β, transitions among the four phases will result.

Based on Eq. (3), we can get the following information when A=D=1 and B=-1:

(1) When $\alpha = 0$, i.e., at the phase of triple points + nodal lines, the locations of the extra nodal lines are $\cos\mathrm{k_z} = D/2B\beta$. Therefore, the extra nodal line shifts to

high k_z when β is increased.

(2) At Γ, $k_z = (\frac{D}{2\alpha B} - \frac{\beta}{\alpha})k_x$, because $k_x \to 0, k_z \to 0$. Therefore, at the nexus phase, the slope of the nodal line is $\frac{D}{2\alpha B}$ because $\beta = 0$. At the nexus network phase, the slope changes its sign with the variation of β.

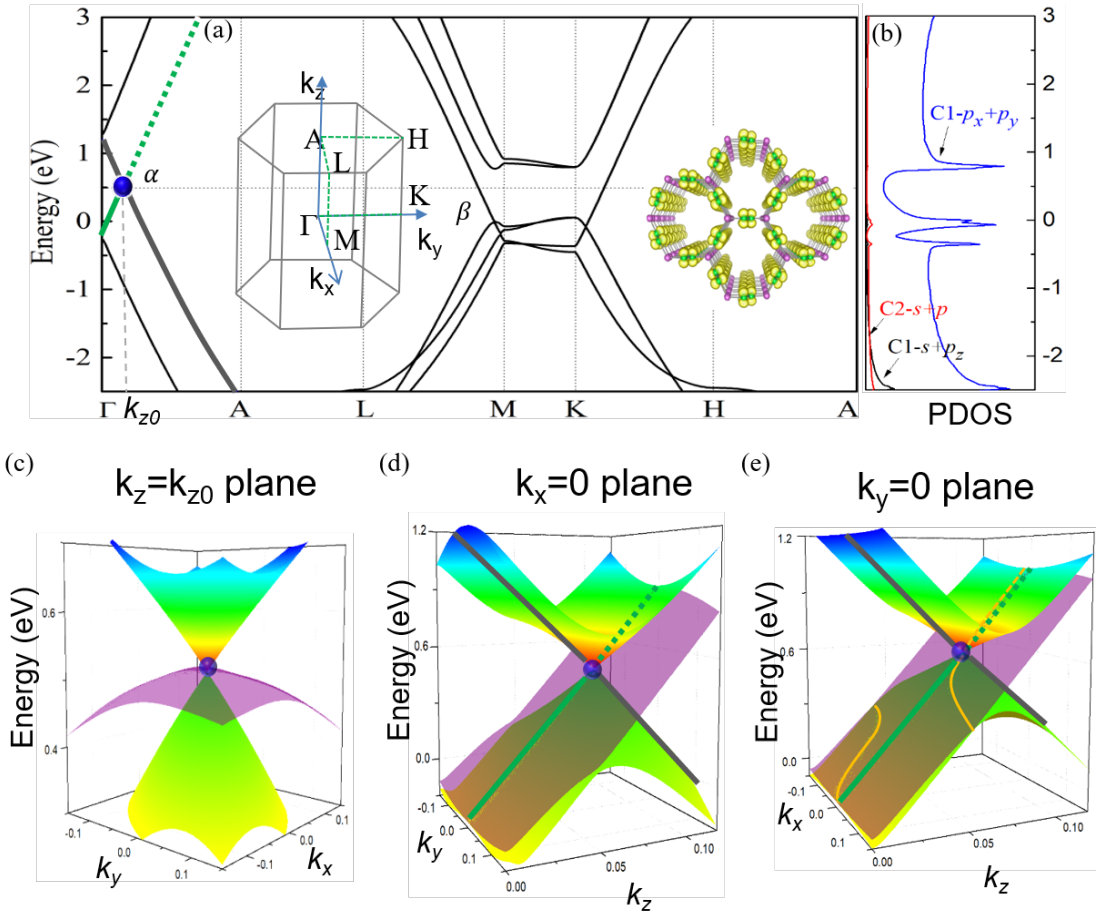

Fig. S1. (a) Band structure of CHC-1. Point α (blue dot at k_z = 0.07 π/c) along Γ – A is a NP, as a result of band crossing between the double degenerate (green) and non-degenerate (red) bands. Inset (left): first BZ and inset (right): charge density contour of a state near α. (b) Partial density of states (PDOS) of CHC-1. (c)-(e) 3D band structures around α with (c) k_z = 0.07 π/c, (d) k_x = 0, and (e) k_y = 0, respectively. The green lines in (d) and (e) are where the tilted (purple) energy surface and the cones intercept. The color and line pattern are the same as in (a). The orange lines in (e) are where additional crossing lines between the energy surface and cones have been registered.

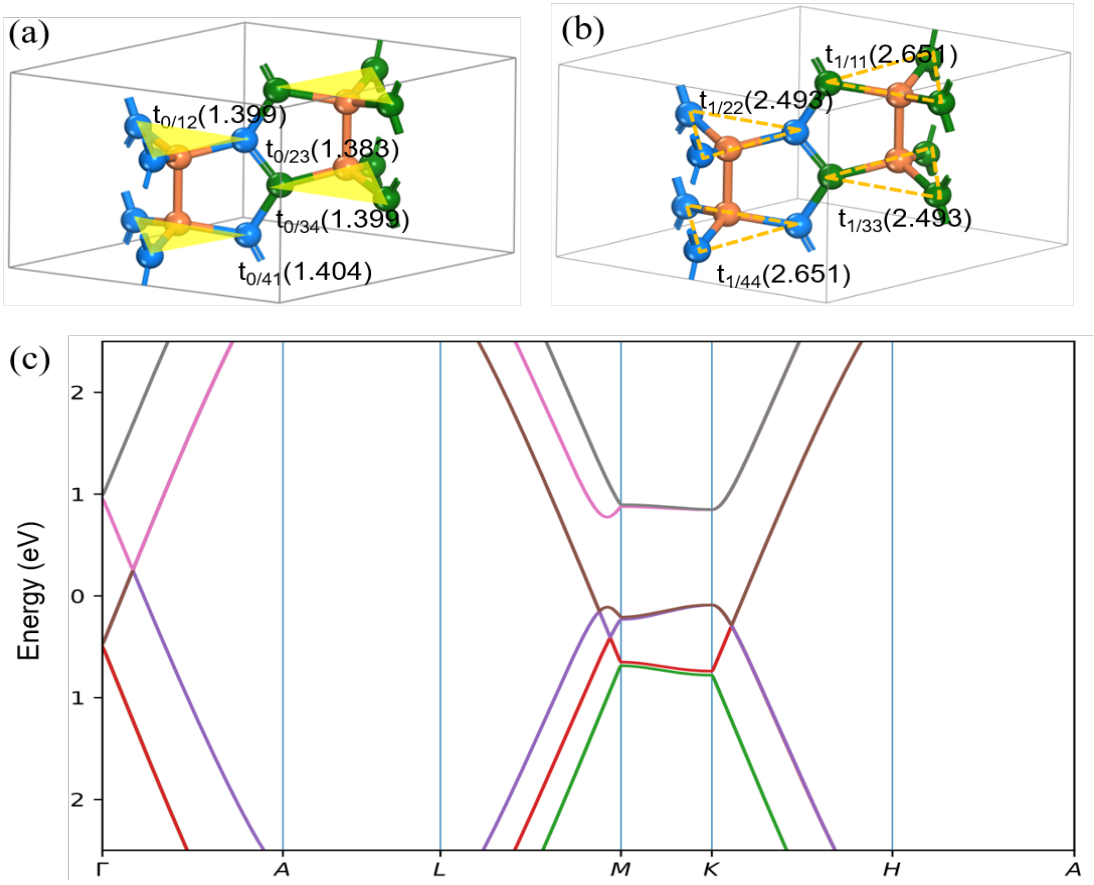

Fig. S2. (a-b) Two example for the tight-binding parameters t_0 and t_1 in the CHC-1. $t_{i/mn}$ (i=0~1, m, n=1~4) is the hopping energy t_i between layers m and n. The yellow triangles in (a) and dashed orange triangles in (b) correspond to four atomic layers in the primitive cell of CHC-1. The values in the parentheses are corresponding bond lengths. (c) Band structure of CHC-1 by using the tight-binding parameters in the last column of Table S2.

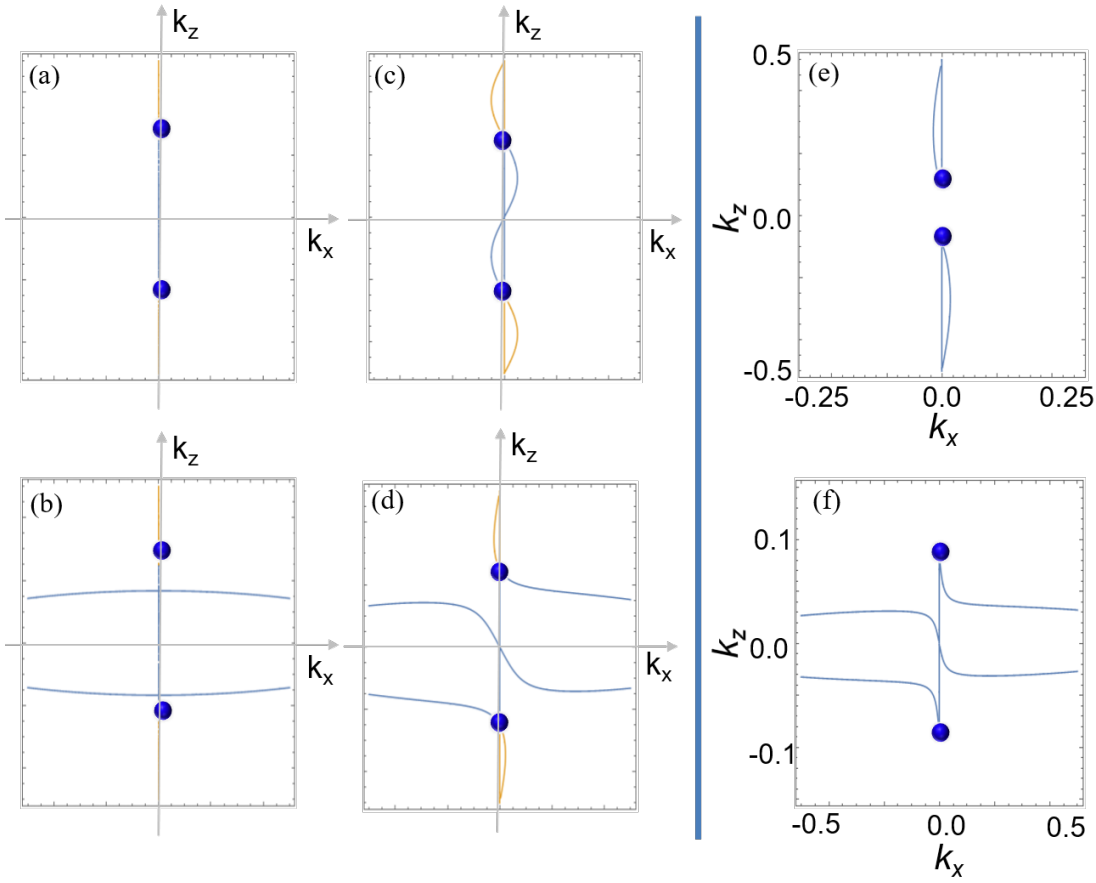

Fig. S3. (a-d) Four topological phases, based on the k·p model in Eq. (2), corresponding to the phases in Figs. 4(a-d), respectively. (a) A TP phase with $\alpha = \beta = 0$; (b) A TP-ANL phase with $\alpha = 0, \beta = -1$; (c) A NP phase with $\alpha = 0.2, \beta = 0$; (d) A nexus network with $\alpha = 0.2, \beta = -1$. The other parameters are $A_1 = 1$, $B_1 = -1$, $A_2 = -1$, $B_2 = 1$, $D = 1$, $C_1 = C_2 = 0$. (e-f) The nexus network similar to those in Figs. 3(d) and 3(e), reproduced by Eq. (2) with $A_1 = -A_2 = 1.45$, $B_1 = -B_2 = -1$, $D = 1$, $C_1 = -C_2 = 0.85$, $\alpha = 0.05$.

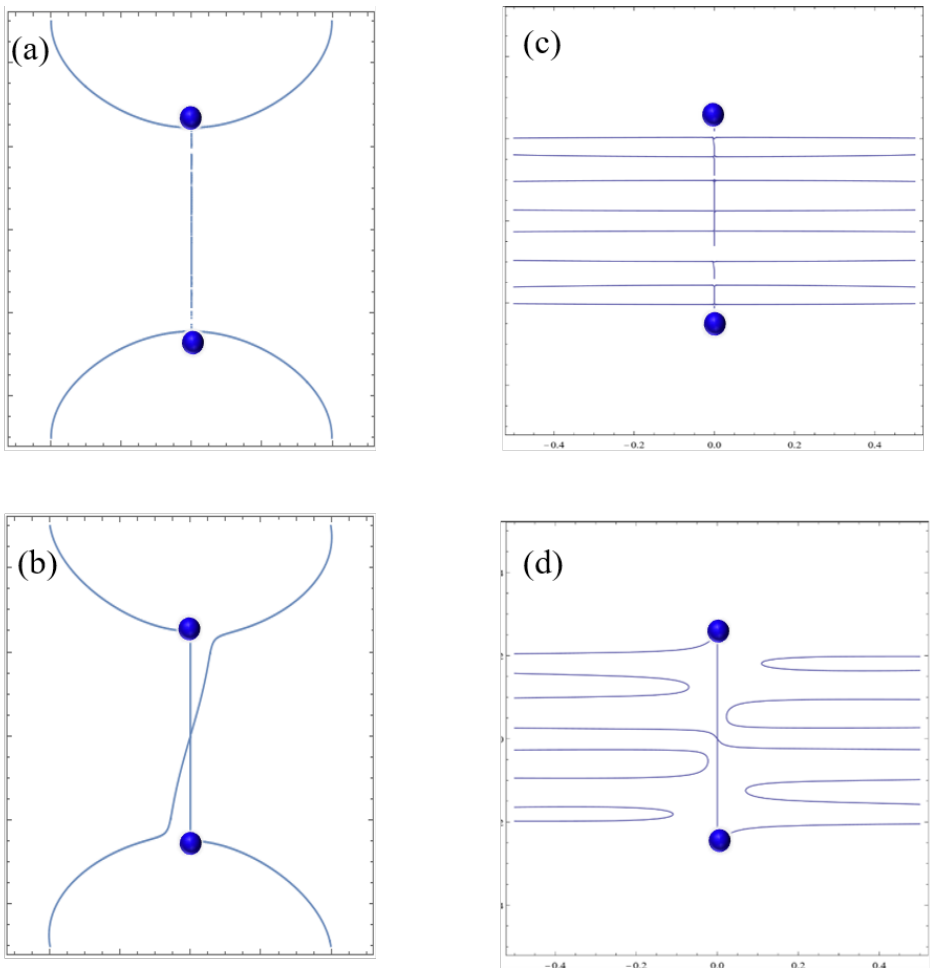

Fig. S4. Other TP-ANL and nexus network based on the $k \cdot p$ model in Eq. (2). (a) TP-ANL phase including two TPs and a nodal ring ($\alpha = 0,\ \beta = -15$); (b) Nexus network evolving from (a) when the TPs transition to NPs ($\alpha = 0.8,\ \beta = -15$); (c) TP-ANL phase including two TPs and additional 8 nodal lines ($\alpha = 0,\ \beta = -1,\ \gamma = 0.5,\ \delta = 12$); (d) Nexus network evolved from (c) when the TPs transition to NPs ($\alpha = 0.1,\ \beta = -1,\ \gamma = 0.5,\ \delta = 12$). For (c) and (d), β in Eq. (2) is replaced by $\beta + \gamma\cos(\delta k_z)$. The other parameters are $A_1 = 1,\ B_1 = -1,\ A_2 = -1,\ B_2 = 1,\ D = 1,\ \ C_1 = C_2 = 0$.

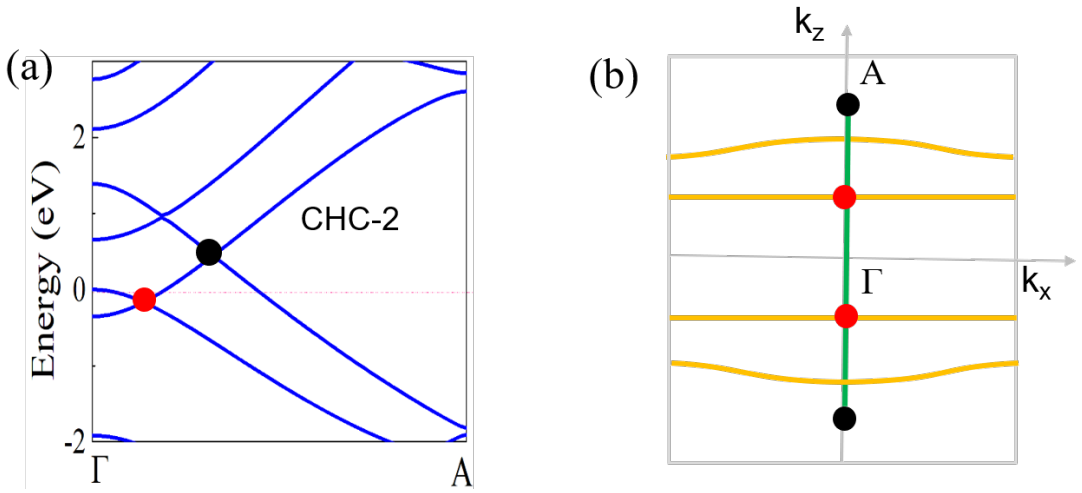

Fig. S5. (a) Band structure along k_z ($\Gamma - A$) for CHC-2, in which there exist a TP (black dot) and a 4-fold degenerate point (red dot). (b) Topological phases of CHC-2 on the plane k_y=0. It is a TP-ANL phase including a TP, a 4-fold degenerate point and additional 4 nodal lines. The TP and 4-fold degenerate point are connected by a trivial (green) nodal lines.

Table S1. Structural parameters of CHC-1, CHC-2 and CHC-1'. The corresponding parameters of CKL, diamond and graphite are also shown for comparison.

Structure	Space group	Lattice parameters		Density	Bond lengths	Bulk Moduli	E_{coh}
		a = b	c				
CHC-1	P-3m1	6.35	4.83	1.89	1.38 ~ 1.64	225.00	-7.57
CHC-1'	$P6_3/mmc$	6.39	2.42	1.87	1.41,1.49	220.77	-7.37
CHC-2	$P6_3/mmc$	10.10	4.86	1.30	1.39 ~ 1.64	155.54	-7.66
CKL	$P6_3/mmc$	4.46	2.53	2.75	1.50,1.53	322	-7.44
Diamond	$Fd\bar{3}m$	3.56	3.56	3.55	1.54	431.32	-7.77
Graphite	$P6_3/mmc$	2.46	6.80	2.24	1.42	36.40	-7.90

Table S2. Tight-binding hopping parameters $t_{i/mn}$ (i=0~5, m, n=1~4) in Eq. (1) for the four phases in Fig. 4, where m and n label the ordinal number of layers (see the explanation in Fig. S2). Parameters in the TP and TP-ANL phases are for the CHC-1' structure, while those in the NP and Nexus network phases are for the CHC-1 structure.

t_i	mn	TP phase	NP phase	TP-ANL phase	Nexus network
t_0	12 or 34	2.8	2.8	2.8	2.8
	23		3.2		3.2
	14		2.4		2.4
t_1	11 or 44	0.45	0.4	0.45	0.4
	22 or 33		0.5		0.5
t_2	11 or 44	0	0	0.15	0.18
	22 or 33				0.12
t_3	11 or 44	-0.045	-0.05	-0.045	-0.05
	22 or 33		-0.04		-0.04
t_4	12 or 34	-0.015	-0.018	-0.015	-0.018
	23		-0.013		-0.013
	14		-0.013		-0.013
t_5	12 or 34	-0.02	-0.025	-0.02	-0.025
	23		-0.013		-0.013
	14		-0.013		-0.013

Table S3. $\mathbf{k}\cdot\mathbf{p}$ model parameters in Eq. (2) for different topological phases in Figs. 4 and 5.

	TP phase in Fig. 4(a)	TP-ANL phase in Fig. 4(b)	NP phase in Fig. 4(c)	nexus network in Fig. 4(d)	Extended TP-ANL phase in Fig. 5(a)	Extended nexus network in Fig. 5(b)
A_1	1	1	1	1	1	1
B_1	-1	-1	-1	-1	-1	-1
C_1	0	0	0	0	0	0
A_2	-1	-1	-1	-1	-1	-1
B_2	1	1	1	1	1	1
C_2	0	0	0	0	0	0
D	1	1	1	1	1	1
$\boldsymbol{\alpha}$	0	0	0.5	0.5	0	0.1
$\boldsymbol{\beta}$	0	-1	0	-1	-1	-1
γ	0	0	0	0	0.5	0.5
δ	0	0	0	0	4	4